Frontiers in Heat and Mass Transfer (FHMT), 19, 35 (2022)
DOI: 10.5098/hmt.19.35

Global Digital Central
ISSN: 2151-8629

Frontiers in Heat and Mass Transfer

Available at www.ThermalFluidsCentral.org

NUMERICAL SIMULATION OF LARGE ARRAYS OF IMPINGING JETS ON A FLAT SURFACE

Ali Chitsazan[a,*] Georg Klepp[a], Birgit Glasmacher[b]

[a]*Institute for Energy Research, Ostwestfalen-Lippe University of Applied Sciences and Arts, Lemgo 32657, Germany*
[b]*Institute for Multiphase Processes, Leibniz University Hannover, Hannover 30167, Germany*

ABSTRACT

The objective of the present research is the prediction of large arrays of impingement jets using a computational model. The heat transfer and the force coefficient from single and multiple jet rows (1, 2, 4, 8, and infinity rows) for two different nozzle shapes as either orifice or straight pipe on a fixed flat surface were numerically investigated for drying applications to understand the physical mechanisms which affect the uniformity of the local heat transfer and pressure force coefficient as well as average heat transfer coefficient. The pipe has always a higher averaged Nu and pressure force coefficient compared to the orifice nozzle. Increasing the nozzle to surface distance and decreasing the jet impingement angle reduces the heat transfer and pressure force coefficient. The local Nu number curves for multiple jet rows exhibited many different shapes because of different interference intensities between adjacent jets and also the magnitude of cross-flow. The impact of multiple jet rows on averaged Nu number and jet force coefficient was negligible compared to the single jet row.

Keywords: *CFD, Jet Impingement, Nozzle Shape, Jet Rows, Heat Transfer, Pressure Force*

1. INTRODUCTION

Multiple impinging jets with different geometries are used in heating, cooling, and drying applications. The degree to which the geometry variations differ is strongly influenced by the S/d, H/d, the magnitude of cross-flow, nozzle shape, number of jet rows, etc. Due to these complicated relations, the numerical consideration of geometry variation is equally important for the suitability of CFD for impingement heat transfer in turbomachinery applications, in which different geometry variation is also commonly found. There are several correlations available in the literature to predict heat transfer (e.g. Martin, 1977; Chitsazan et al., 2022).

The heat transfer has no dependence on the number of jet rows in a spanwise direction if the spanwise jet-to-jet spacing is large. For arrays of smaller spanwise jet-to-jet distance, due to the associated more powerful crossflow, the heat transfer rate is considerably more dependent upon the number of jet rows in the spanwise direction and the heat transfer rate in the spanwise direction is lower. Consequently, the reduction of the spanwise jet-to-jet distance by increasing the number of jet rows in the spanwise direction degrades the average heat transfer rates, especially at large H/d (Behbahani and Goldstein, 1983; Hollworth and Cole, 1987). Kumar and Prasad (2008) found experimentally that five jet rows have the best performance compared to the single jet row and the single jet on a concave surface. Li and Corder (2008) showed that the peak value of local heat transfer for dual impinging jets is higher than a single jet. The dual impinging jets provide a higher average heat transfer around the stagnation region. Bu et al. (2015) observed only one peak in the local Nu distribution for three rows of jets due to strong interference between adjacent jets. Patil and Vedula (2015) found that the single jet row has higher Nu compared to two jet rows with the same mass flow rate.

On the other hand, Ashforth-Frost and Jambunathan (1996) reported that the shape of jet exit geometry also plays an important role in impinging jet development.

The computational analysis of multiple impinging jets is generally based on the solution of the Navier-Stokes equations. Direct numerical simulations are still limited to the single jet or small Re (Suzuki *et al.*, 2018). The large-eddy simulation was performed to better understand the complex flow of multiple jets, although these simulations are expensive (Draksler *et al.*, 2017). Reynolds-averaged Navier-Stokes equations with an appropriate turbulence model such as the SST k-omega turbulence model are computationally less expensive and are recommended by several researchers as the best compromise between computational cost and accuracy (Zuckerman and Lior, 2006; Chitsazan et al., 2021).

As most studies have experimentally considered the array configurations with relatively few numbers of impinging jets and rows on the impingement heat transfer also these works focus only on the curved surface and there is no investigation of the impact of pressure force. A global pressure force on the surface is typical for impinging jets towards the surface and it is very important in drying applications for force-sensitive products such as paper. The nozzle exit velocity could be limited if the product is sensitive to deformation under the jet impinging force. The objective of the present research is the prediction of large arrays of impingement jets using a computational model. The analysis includes the effect of different nozzle shapes (orifice and long pipe) and the number of jet rows (1, 2, 4, 8, and infinity rows) on the heat transfer and pressure force to understand the physical mechanisms which affect the uniformity of the local and average heat transfer coefficient, and pressure force coefficient.

* *Corresponding author. Email: ali.chitsazan@yahoo.com*

Global Digital Central
ISSN: 2151-8629

2. COMPUTATIONAL DOMAIN, GRID, AND VALIDATION

As the first case for investigation, the multiple jets with one row in the inline arrangement is considered, and the number of jets is assumed infinity as shown in Fig.1. The jet-to-jet spacing (S) in both directions of space was 7.2d and the distance between the target surface and the jets (H) was 5.4d. These geometrical parameters are reported by Martin (1977) for an optimum design. For numerical treatment, due to the symmetric geometry, the problem was simplified according to the schematic shown in Fig. 2.

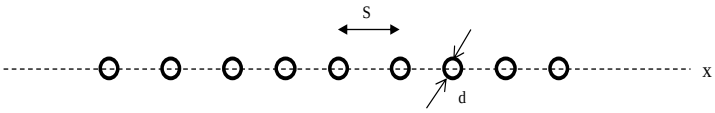

Fig. 1 Details of holes arrangement; Single row of jets

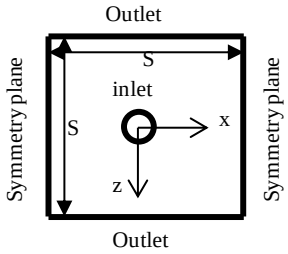

Fig. 2 Schematic of the computational domain; Top view of confinement surface

The numerical setup is built up and run with the commercial code STAR-CCM+. The k-omega SST model was used to describe turbulence. Polyhedral mesh type was generated and the final numerical model accounted for about 2,328,819 grid cells as shown in Figure 3. Please refer to Chitsazan and Glasmacher, 2020 for more detail.

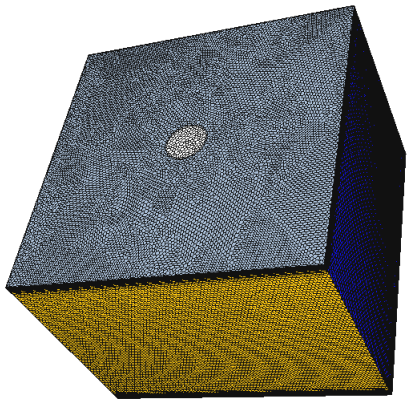

Fig. 3 Three-dimensional view of the grid generation

The mesh sensitivity analysis was conducted for a high Re value (Re= 23000) to estimate the maximum error as shown in Table 1. The local discretization error distribution is calculated by the grid convergence index (GCI) method (Roache 1994 and 2003). The overall discretization error for the fine and coarse grid was very small. The intermediate grid is selected as the final grid to reduce the computational cost (see Figure 4 and Table 1).

Table 1 Grid parameters of the sensitivity study

Grid	Base size (m)	Cell number	Max y_1^+	Average GCI %
Course	0.000395	476561	0.493	---
Intermediate	0.000285	1049923	0.507	2.3
Fine	0.000205	2328819	0.510	1.65

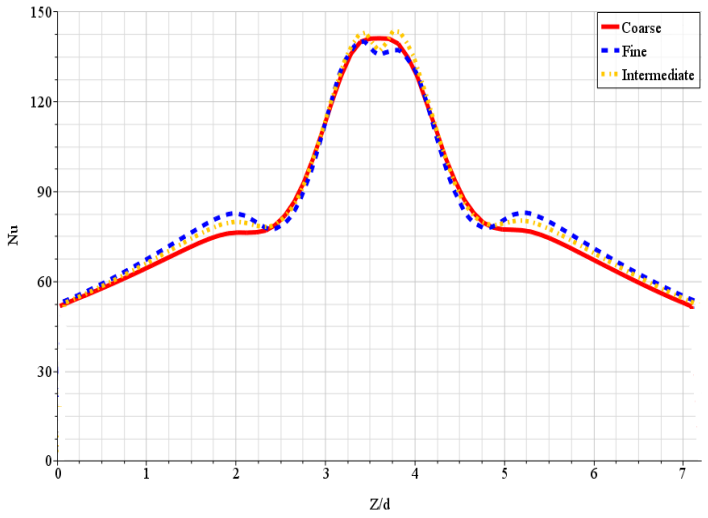

Fig. 4 Nu distribution in the grid sensitivity study

Fig.5 compares the results of numerical simulation with Martin's correlation (Martin 1977). The heat transfer depends on the jet Reynolds number (Re) and the average Nu increases as the Re increases. The difference between the CFD and correlation is approximately 13% on average and closely followed the same trend. Differences in nozzle arrangement and upstream flow conditions influence the comparison.

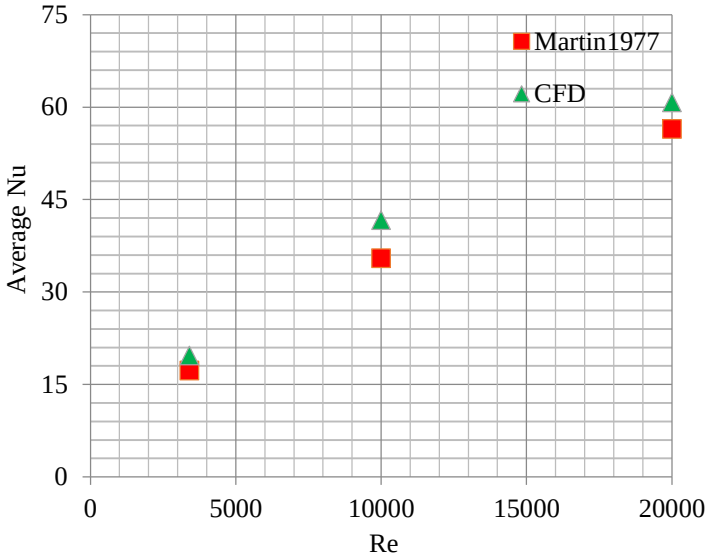

Fig. 5 Comparison of average Nu from CFD and literature at H/d = 5.4, S/d=7.2 for different Re on a logarithmic scale

3. RESULTS AND DISCUSSION

3.1 Variation of Nozzle Shapes and Number of Jet Rows

3.1.1 Effect on Heat Transfer

The effect of geometry variation i.e. the nozzle shapes and the number of jet rows is addressed. The jet nozzle shape has a role in the development of an impinging jet and also the number of jet rows has an important role in the magnitude of the cross-flow. The degree to which these geometry variations differ is strongly influenced by the jet-to-jet spacing, the separation distance, and the magnitude of cross-flow. Due to these complicated relations, the numerical consideration of geometry variation is equally important for the suitability of CFD for the impingement heat transfer in turbomachinery applications, in which different geometry variation is also commonly found.

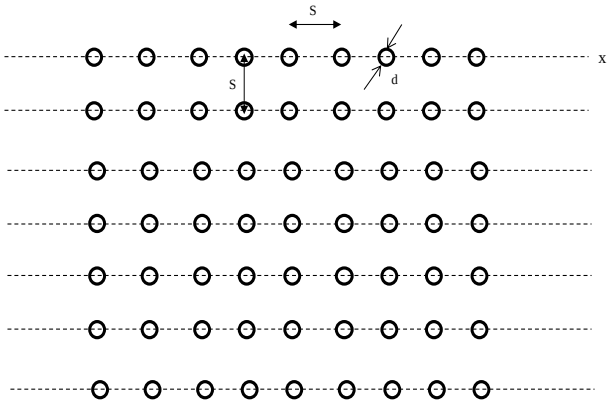

Case 1 (a) Infinity rows of jets, Nozzle: pipe

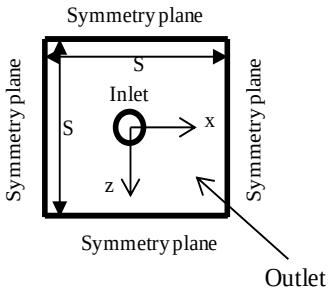

Case 1 (b) Schematic of the computational domain for case 1

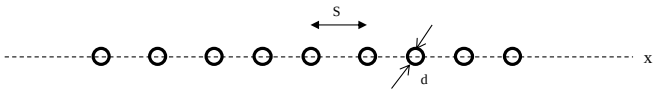

Case 2 (a) Single row of jets; Nozzle: orifice or pipe

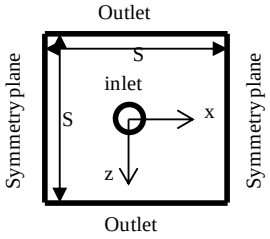

Case 2 (b) Schematic of the computational domain for case 2

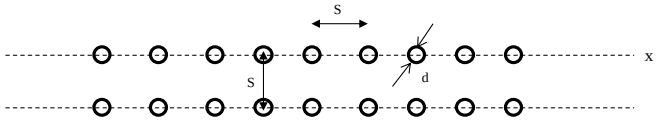

Case 3 (a) Two rows of jet; Nozzle: orifice or pipe

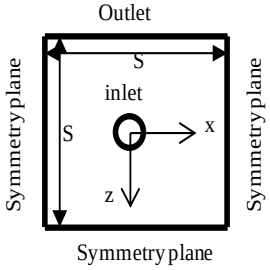

Case 3 (b) Schematic of the computational domain for case 3

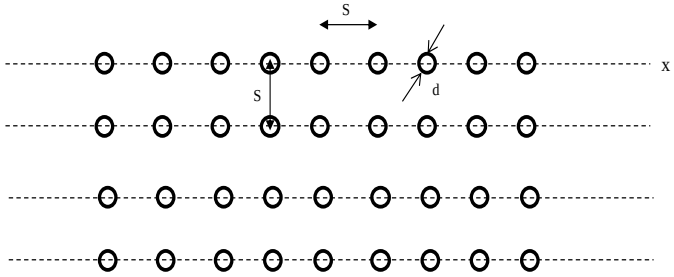

Case 4 (a) Four rows of jet; Nozzle: orifice or pipe

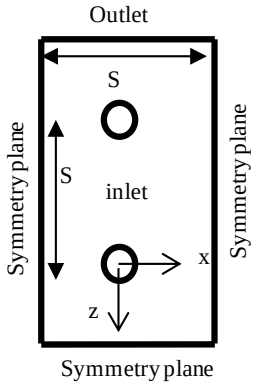

Case 4 (b) Schematic of the computational domain for case 4

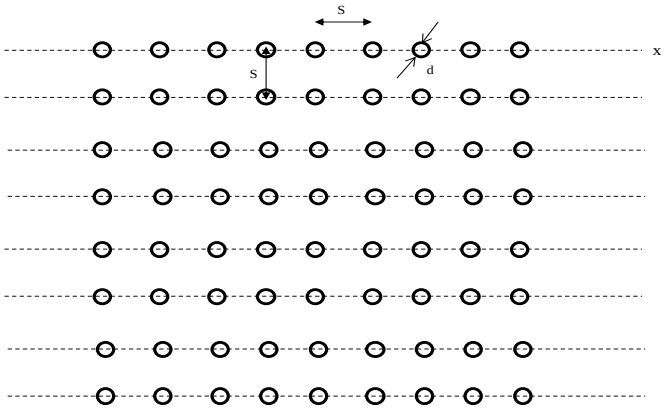

Case 5 (a) Eight rows of jet; Nozzle: orifice or pipe

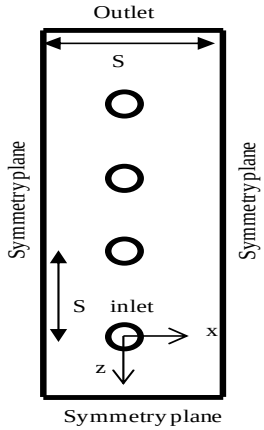

Case 5 (b) Schematic of the computational domain for case 5a

Fig. 6 Details of nozzle arrangement and schematic of the computational domain (top view of confinement surface)

Global Digital Central
ISSN: 2151-8629

In the present study the two commonly used nozzle types, i.e., straight round pipe and the round orifice are selected. In the present cases, the pattern was regular with S = 7.2d. Data was taken for Re = 10000, H/d = 5.4. These geometrical parameters are reported by Martin (1977) for an optimum design. In all cases the diameter of the nozzles (d) was equal. As already mentioned, all jet inlets of orifice nozzles were modeled as circular planes. The ratio of pipes' length to diameter is 10 to obtain a fully developed jet flow. Two-dimensional numerical calculation models of impinging jets of orifice and pipe nozzles with the boundary conditions are presented in Fig. 6. Multiple jets with different numbers of rows in the inline arrangement are considered and the number of jets is assumed to infinity according to the schematic shown in Fig. 6 (left sides). For numerical treatment, due to the symmetric geometry, the problem was simplified according to the schematic shown in Fig. 6 (right sides).

Figure 7 compare the centerline Nu distributions from CFD for the different nozzle arrangement. Based on comparisons with the Nu functions for the pipe nozzle array, it is evident from Figure 7 that the peak of local Nu at the stagnation region of pipe nozzles and also the average value of Nu number on the target surface is higher than that of the orifice nozzle (see Figure 9). Because for the same Re, pipe nozzles effectively have a higher initial core velocity resulting in higher heat transfer at the impingement point (see figure 8). For cases 4 and 5, the flow within such a large array of impinging jets is quite complex due to the crossflow effects and there is not observed a significant difference in the total average Nu number on the target surface between these cases. However, In the case of orifice nozzle, the heat transfer is somewhat less but they are the easiest to manufacture and consequently are commonly used. This observation correlates with the finding of Ansu et al. (2016).

Figure 8 shows the velocity contours along the symmetry plane for different nozzle arrangements and shapes. As each fluid jet ejects out of the pipe with a parabolic velocity profile and out of the orifice with a fairly flat velocity profile, a continuous reduction in velocity takes place from the exit nozzle to the outer boundary. The flow is strongly affected by the presence of the impingement surface which creates the stagnation point region. The wall jet region is characterized by flow directed radially outwards and the wall parallel velocity component is then accelerated from zero to a maximum value. Increasing the jet exit velocity from the nozzle leads to increasing the pressure and heat transfer at the stagnation point (Chitsazan and Glasmacher, 2020).

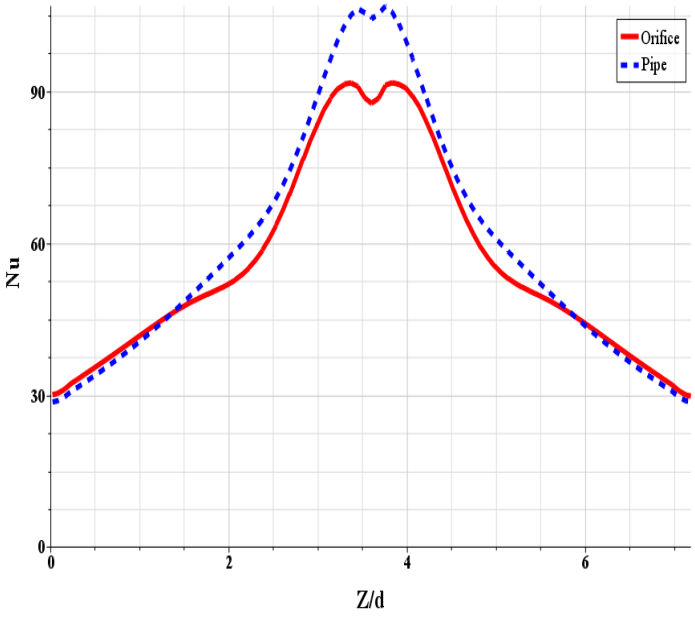

(a) Number of rows: One

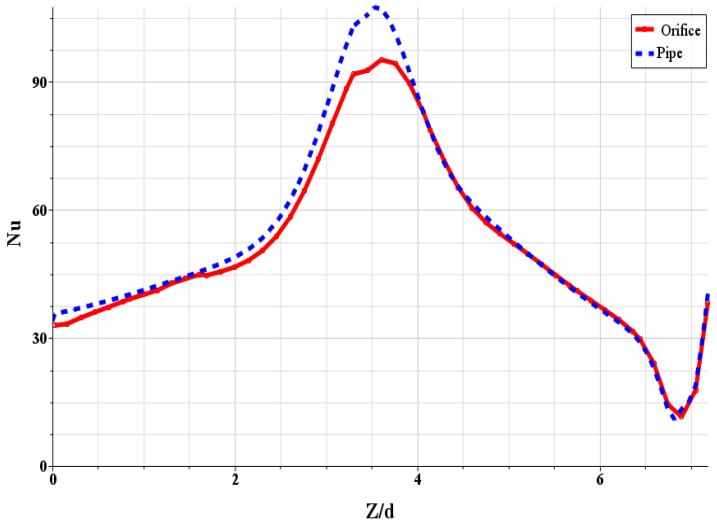

(b) Number of rows: Two

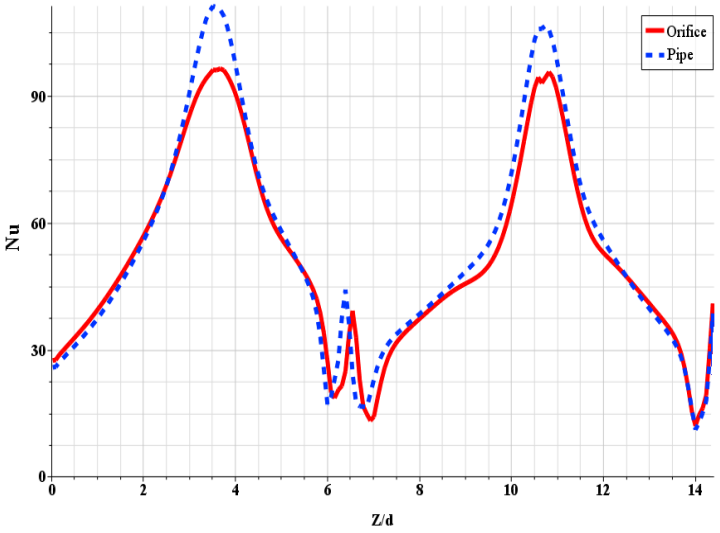

(c) Number of rows: Four

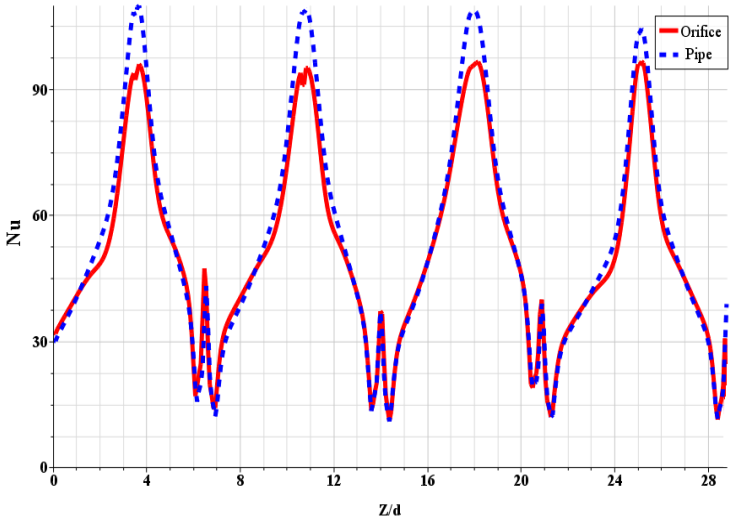

(d) Number of rows: Eight

Fig.7 Comparison of centerline Nu distributions from CFD for different nozzle arrangements and shapes at H/d = 5.4, S/d=7.2, Re=10,000

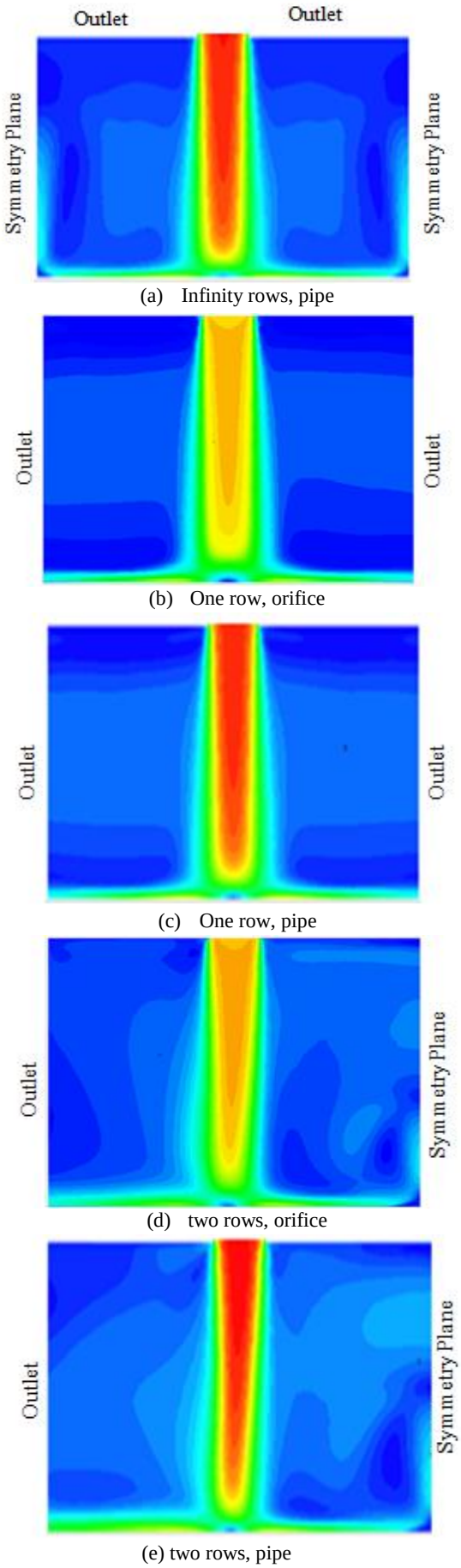

(a) Infinity rows, pipe

(b) One row, orifice

(c) One row, pipe

(d) two rows, orifice

(e) two rows, pipe

(f) Four rows, orifice

(g) Four rows, pipe

(h) Eight rows, orifice

(i) Eight rows, pipe

Fig. 8 Velocity magnitude contours along symmetry plane for different nozzle arrangements and shapes at S/d=7.2, Re=10,000, H/d = 5.4

Global Digital Central
ISSN: 2151-8629

Figure 9 compare the total average Nu from CFD for different nozzle arrangement and shapes. It is found that Case 1 (infinity rows), where the air jets exit through the top side after impingement provides the highest values of the total average Nu on the entire target surface compared to other cases. Because for case 1 (infinity rows), the exit opening area is the least for this configuration and the momentum exchange between the fluid jet and ambient is minimum. Case 2 (single row, either pipe or orifice) provides the highest Nu after case 1. This is due to the symmetrical distribution of velocity around the jet axis. Since there is no cross flow and the jet hits the target surface without any distortion (See Fig. 8 a,b,c).

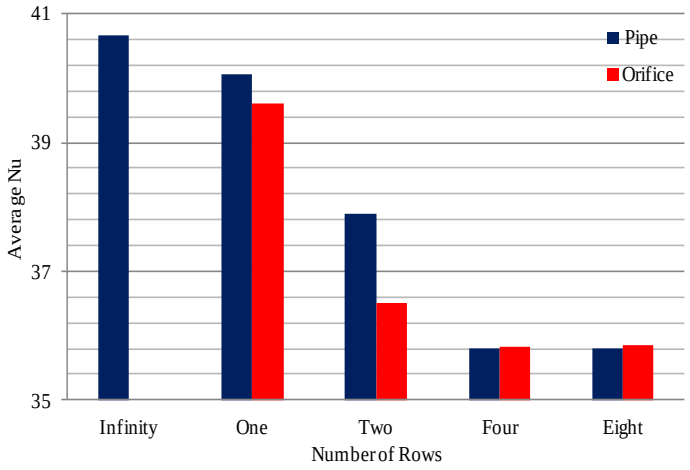

Fig. 9 Comparison of total average Nu from CFD for different nozzle arrangements and shapes at S/d=7.2, Re=10,000, H/d = 5.4

It is found that, for multiple row cases (2, 4, and 8 rows), the wall jet interference and crossflow effects cause significant degradation of the averaged Nu number when compared to the single row. The flow is quite complex within such a large array of impinging jets due to the crossflow effects. The strength of crossflow increases along the channel and therefore the last jet in the channel experiences the maximum crossflow. The presence of the crossflow will thicken the wall boundary layers, disturb the jet flow pattern, and degrade the heat transfer rates. On the other hand, the wall jets from the adjacent jets when interacting with each other result in an upward fountain as shown in Figure 8 (d)-(i). The presence of the fountain can cause the recirculating flow region and the thermal exchange occurring between the recirculating flow and the impingement surface harm the impingement surface heat transfer. However, where these wall jets impinge upon each other, there may occur secondary stagnation regions (see Figures 7 b, c, and d).

Two rows case (either pipe or orifice) provides the higher Nu compared to Case 4 and 5 because of the weaker crossflow and wall jet interference effects (see Fig. 8 (d)-(i)).

For eight rows (either pipe or orifice) the magnitude of the total average Nu on the target surface remains the same compared to the four rows due to the same flow pattern and mass flow rate per unit surface area.

3.1.2 Effect on Pressure Force

Figures 10 show the distributions of pressure for different nozzle shapes and the number of jet rows on the target surface. Figure 11 shows the comparison of pressure force coefficient from CFD for different nozzle arrangements and shapes.

The pressure has the maximum value at the 1st stagnation point and reduces as the flow accelerated in the wall jet region, for all the cases. Based on comparisons with the pressure for the pipe nozzle array, it is evident from Figure 10 that the peak of pressure at the stagnation region of pipe nozzles is higher than that of the orifice nozzle. Because the pipe nozzles have a higher initial core velocity resulting in a higher stagnation pressure for the same Re. That's why in the case of orifice nozzle the pressure force is somewhat less but they have a high potential in drying application for a force-sensitive product also they are the easiest to manufacture and consequently are commonly used.

For infinity rows, where the air jets exit through the top side after the impingement and also the single row (either pipe or orifice) where the flow exits in both directions after impingement, provide the highest values of the stagnation pressure and subsequently the pressure force coefficient on the entire target surface compared to the other cases. This is due to the symmetrical distribution of pressure around the stagnation point (see Figures 10 a, b, c). On the other hand, there is no significant difference in the pressure force coefficient between the single row (pipe) and the infinity rows (see Fig. 11).

It is found that, for multiple row cases (2, 4, and 8 rows), the wall jet interference and crossflow effects cause a significant effect on the pressure force coefficient when compared to the single row. The strength of crossflow increases along the channel and the last jet experiences the maximum crossflow. The crossflow will disturb the jet flow pattern and degrade the stagnation pressure. There may occur the secondary stagnation region in the up-wash fountain zone as shown in Figure 10 (g). The fountain can cause the recirculating flow and affect the impinging jet flow behavior. Therefore, the pressure force coefficient from multiple row cases (2, 4, and 8 rows) is lower than the single row. This could be attributed to the strong wall jet interference and crossflow effect for multiple rows compared to the single row.

The stagnation region has the strongest pressure for both single and multiple-row cases. However, it is observed that the peak Nu values for multiple row cases (2, 4, and 8 rows) increase as the number of jet rows increases from 2 to 8. This slight difference is due to the much larger interaction of the multiple row cases before impingement increases the turbulence in the flow and thus increases the pressure and consequently the pressure force at the stagnation region. Therefore, the pressure force coefficient increases as the number of jet rows increase from 2 to 8 and this matter is more obvious for the pipe nozzles.

The pipe has always a higher average Nu and the pressure force coefficient compared to the orifice nozzle and the maximum difference is around 12% and 24% respectively. The orifice nozzle seems to have a high potential in industrial drying applications for a force-sensitive product. The impact of multiple rows with regards to the heat transfer and pressure force is negligible compared to the single row within the range examined and the maximum difference is around 10% and 8% respectively. This could be attributed to the strong wall jet interference and crossflow effect for multiple rows compared to the single row.

4. CONCLUSION

Within this paper, the number of jet rows and the nozzle shapes of multiple impinging jets was investigated. The consideration of large arrays was of particular interest as most studies in the present literature have considered array configurations with relatively few numbers of impinging jets. In the computations, the numerical simplification allowed a substantial reduction of the problem size. In the course of this paper, the effects of single and multiple rows were discussed to understand the physical mechanisms which affect the uniformity of the local and average heat transfer, and jet force from the single row and multiple rows. For this, the average Nu was compared with experimental data. The overall agreement found was good for the prediction of complex configurations by using reasonably simplified problems. The pipe has always a higher averaged Nu number and pressure force coefficient compared to the orifice nozzle. Nu number curves for multiple jet rows exhibited many different shapes compared to the single row because of different interference intensities between adjacent jets and also the magnitude of cross-flow. The impact of multiple jet rows on heat transfer and pressure force was negligible compared to the single row by approximately 9 and 13% on average.

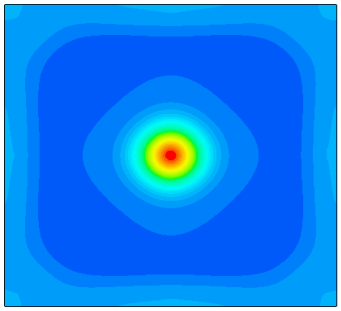

(a) Infinity Rows, Pipe

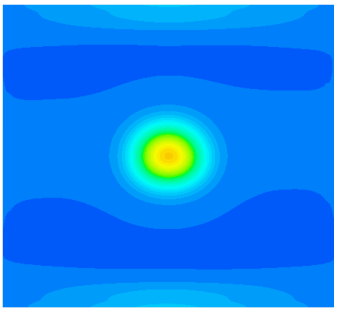

(b) One Row, Orifice

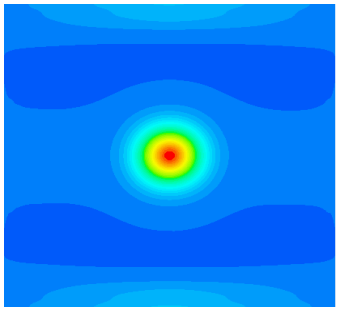

(c) One Row, Pipe

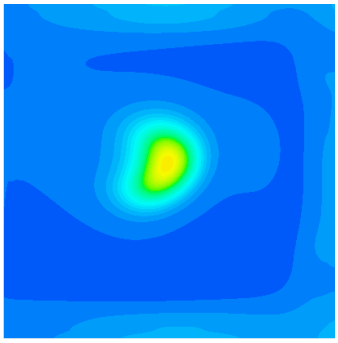

(d) Two Rows, Orifice

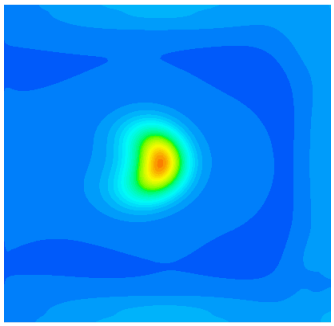

(e) Two Rows, Pipe

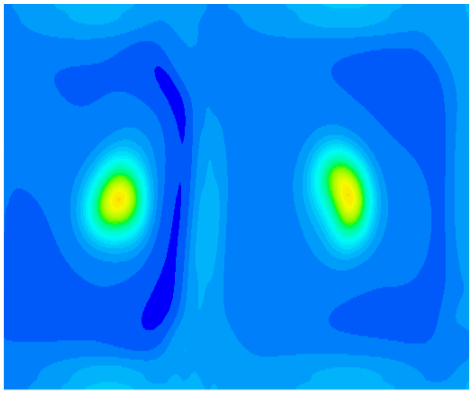

(f) Four Rows, Orifice

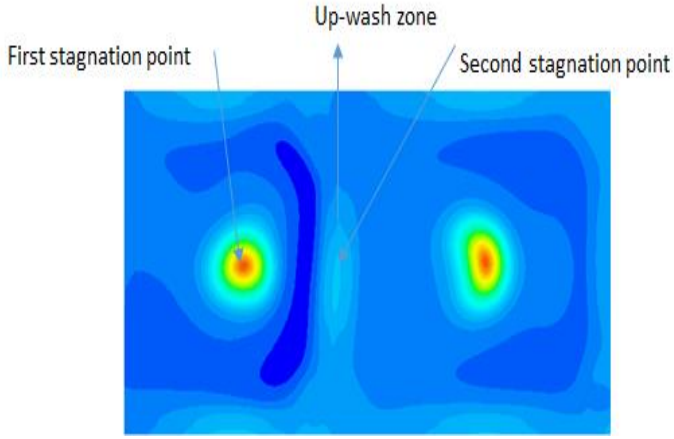

(g) Four Rows, Pipe

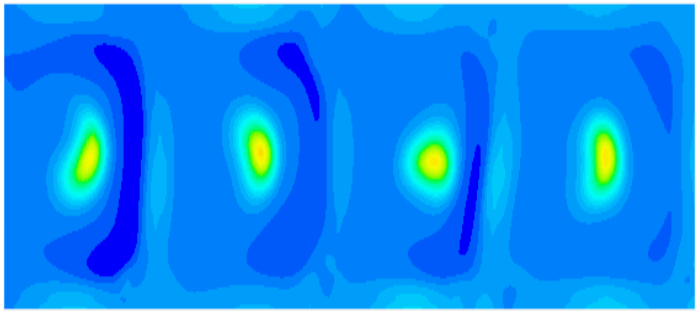

(h) Eight Rows, Orifice

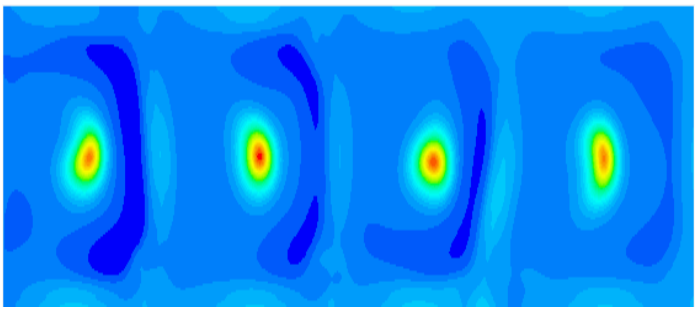

(i) Eight Rows, Pipe

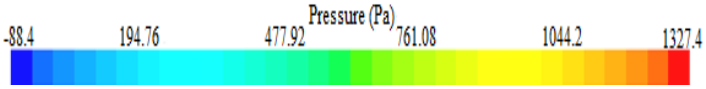

Fig. 10 Pressure distribution on a target surface

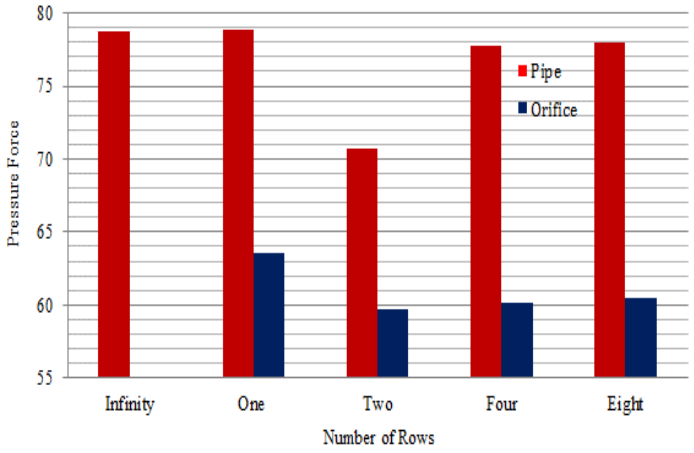

Fig. 11 Comparison of pressure force coefficient from CFD for different nozzle shapes and number of jet rows at S/d=7.2, Re=10,000, H/d = 5.4

NOMENCLATURE

A	surface area (m^2)
C_f	force coefficient $P_{st}A \big/ 0.5\rho V^2(\pi d^2/4)$
d	jet diameter (m)
F	force (N)
H	nozzle-to-target spacing (m)
k_t	Fluid thermal conductivity (W/m·K)
Nu	Nusselt number $(q/T_w - T_j)\frac{d}{k_t}$
P	pressure (pa)
q	convective heat flux (W/m^2)
Re	Reynolds number
S	jet pitch (m)
S/d	dimensionless spacing between jets
T	temperature (K)
V	magnitude of jet exit velocity (m/s)
y^+	dimensionless wall distance

Greek Symbols

k	turbulence kinetic energy (kgm^2/s^2)
ω	specific dissipation rate of turbulence kinetic energy (1/s)
ρ	density of the fluid (kg/m^3)

Subscripts

ave	average
J	jet
st	stagnation point
w	wall

Abbreviation

CFD	computational fluid dynamic
GCI	grid convergence index
SST	shear stress transport

REFERENCE

Ansu U., Godi S.C., Pattamatta A., Balaji C., 2016, Experimental investigation of the inlet condition on jet impingement heat transfer using liquid crystal thermography. *J. Experimental Thermal and Fluid Science*, 80, 363-375. https://doi.org/10.1016/j.expthermflusci.2016.08.028

Ashforth-Frost S. and Jambunathan K., 1996, Effect of nozzle geometry and semi-confinement on the potential core of a turbulent axisymmetric free jet. *International Communications in Heat and Mass Transfer*, 23, 155-62. https://doi.org/10.1016/0735-1933(96)00001-2

Behbahani, A. I., and Goldstein, R. J., 1983, Local Heat Transfer to Staggered Arrays of Impinging Circular Air Jets. *Journal of Engineering for Power*, 105, 354–360. https://doi.org/10.1115/1.3227423

Bu X., Peng L., Lin G. et al. (2 more authors), 2015, Experimental study of jet impingement heat transfer on a variable-curvature concave surface in a wing leading edge. J. Heat and Mass Transfer, 90, 92-101. https://doi.org/10.1016/j.ijheatmasstransfer.2015.06.028

Chitsazan A., Glasmacher B., 2020, Numerical investigation of heat transfer and pressure force from multiple jets impinging on a moving flat surface. *J. Heat and Technology*, 38, 601-610. https://doi.org/10.18280/ijht.380304

Chitsazan A., Klepp G., Glasmacher B., 2021, Review of jet impingement heat and mass transfer for industrial application. *J. Heat Transfer Research*, 52, 61–91. https://doi.org/10.1615/HeatTransRes.2021038056

Chitsazan A., Klepp G., Glasmacher B., 2022, Correlation development for jet impingement heat transfer and force on a moving curved surface. *J. Frontiers in Heat and Mass Transfer*, 18, 1-9. https://doi.org/10.5098/hmt.18.16

Draksler M., Koncar B., Cizelj L, Niceno B., 2017, Large Eddy Simulation of multiple impinging jets in hexagonal configuration – Flow dynamics and heat transfer characteristics. *J. Heat Mass Transfer*, 109, 16-27. https://doi.org/10.1016/j.ijheatmasstransfer.2017.01.080

Hollworth, B. R. and Cole, G. H., 1987, Heat transfer to arrays of impinging jets in a crossflow. *J. Turbomachinery*, 109, 564–571. https://doi.org/10.1115/1.3262149

Kumar, B. V. N. R., and Prasad, B. V. S. S. S., 2008, Experimental investigation of flow and heat transfer for single and multiple rows of circular jets impinging on a concave surface. *ASME Paper No. GT2008-51044*. https://doi.org/10.1115/GT2008-51044

Li, X. C., and Corder, P., 2008, Characteristics of cooling of the leading edge with a row of dual impinging jets, *ASME Paper No. HT2008-56347*. https://doi.org/10.1115/HT2008-56347

Martin, H., 1977, Heat and mass transfer between impinging gas jets and solid surfaces. *J. Advances in heat transfer*, 13, 1-60. https://doi.org/10.1016/S0065-2717(08)70221-1

Patil V. S. and Vedula R. P., 2015, Heat transfer with single and two rows of axisymmetric jets impinging on a concave surface. *1st International ISHMT-ASTFE Heat and Mass Transfer Conference*, Thiruvananthapuram, India.

Roache, P. J., 1994, A method for uniform reporting of grid refinement studies. *J. Fluids Engineering*, 116, 405–413. https://doi.org/10.1115/1.2910291

Roach, P. J., 2003, Conservatism of the grid convergence index in finite volume computations on steady-state fluid flow and heat transfer. *J. Fluids Engineering*, 125, 731–735. https://doi.org/10.1115/1.1588692

SuzukiT., Tsujimoto K., Shakouchi T., Ando T., 2018, DNS of flow and heat transfer characteristics of multiple impinging jets. *21st Australian Fluid Mechanics Conference*, Adelaide, Australia.

STAR-CCM+ 13.02.013 user guide by CD-Adapco.

Zuckeman, N., Lior, N., 2006, Jet impingement heat transfer: physics, correlaions, and numerical modeling. *J. Advances in heat transfer*, 39, 565-631. https://doi.org/10.1016/S0065-2717(06)39006-5